Kindlin-2 directly binds actin and regulates integrin outside-in signaling

Kamila Bledzka,* Katarzyna Bialkowska,* Khalid Sossey-Alaoui, Julia Vaynberg, Elzbieta Pluskota, Jun Qin, and Edward F. Plow

Department of Molecular Cardiology, Lerner Research Institute, Cleveland Clinic, Cleveland, OH 44195

Reduced levels of kindlin-2 (K2) in endothelial cells derived from $K2^{+/-}$ mice or C2C12 myoblastoid cells treated with K2 siRNA showed disorganization of their actin cytoskeleton and decreased spreading. These marked changes led us to examine direct binding between K2 and actin. Purified K2 interacts with F-actin in cosedimentation and surface plasmon resonance analyses and induces actin aggregation. We further find that the F0 domain of K2 binds actin. A mutation, LK^{47}/AA, within a predicted actin binding site (ABS) of F0 diminishes its interaction with actin by approximately fivefold. Wild-type K2 and K2 bearing the LK^{47}/AA mutation were equivalent in their ability to coactivate integrin αIIbβ3 in a CHO cell system when coexpressed with talin. However, K2-LK^{47}/AA exhibited a diminished ability to support cell spreading and actin organization compared with wild-type K2. The presence of an ABS in F0 of K2 that influences outside-in signaling across integrins establishes a new foundation for considering how kindlins might regulate cellular responses.

Introduction

The kindlin family of cytoskeletal proteins has received considerable attention recently for its capacity to regulate the function of integrin adhesion receptors (Shi et al., 2007; Larjava et al., 2008; Ma et al., 2008; Montanez et al., 2008; Meves et al., 2009; Plow et al., 2014). In mammals, there are three kindlins (kindlin-1, -2, and -3), each encoded by a separate gene. Human diseases that arise from the deficiencies of kindlin-1 (Jobard et al., 2003; White and McLean, 2005) or kindlin-3 (Kuijpers et al., 2009; Malinin et al., 2009; Svensson et al., 2009) have been attributed to disruption of extracellular matrix–integrin–actin networks (Mory et al., 2008; Ussar et al., 2008). Ablation of kindlin-2 (K2; *FERMT2*), the most broadly distributed of the three kindlins, is lethal early in mouse embryonic development (Montanez et al., 2008; Dowling et al., 2008a) and is associated with severe cardiac dysfunction in zebrafish (Dowling et al., 2008a). K2 is found in the focal adhesions (FAs) of adherent cells, including endothelial, skeletal, and cardiac muscle cells (Ma et al., 2008; Dowling et al., 2008b). At these locations, K2 is believed to participate in linking integrins to the actin cytoskeleton (Ussar et al., 2006; Meves et al., 2009).

Kindlins are *FERM*-containing proteins containing N-terminal F0 subdomains preceding the typical F1, F2, and F3 subdomains (Malinin et al., 2010) and have a PH subdomain inserted within their F2 subdomains as a signature feature. A major known function of kindlins depends on their binding to integrins, which can be severely dampened by mutation of QW^{615} to AA in the F3 subdomain of K2 (Ma et al., 2008; Montanez et al., 2008; Xu et al., 2014). Lipid binding to the PH domain and a second site in F0 helps to target K2 to membranes (Metcalf et al., 2010; Liu et al., 2011, 2012; Qu et al., 2011; Perera et al., 2011).

Both kindlin and talin must bind to the β cytoplasmic tail for optimal integrin activation (Plow et al., 2014), but the mechanism for their cooperation to induce inside-out signaling across integrins remains unresolved. Kindlins also have been implicated in outside-in signaling across integrins (Montanez et al., 2008; Feng et al., 2012; Xue et al., 2013). Many actin-binding proteins contain FERM domains, and coexistence of phospholipid- and actin-binding domains within the same molecule allows FERM and ERM proteins to link the plasma membrane and actin (Bretscher, 1983; Pakkanen et al., 1987; Tsukita et al., 1989; Algrain et al., 1993). Talin, which contains the FERM domain with highest homology to the kindlin FERM domain (Ali and Khan, 2014), contains three actin binding sites (ABSs), one located within its FERM domain (Hemmings et al., 1996; Lee et al., 2004; Gingras et al., 2008, 2010).

Although the association of K2 with FA and the actin cytoskeleton has been observed microscopically (Tu et al., 2003; Shi et al., 2007; He et al., 2011), this interaction is assumed to be indirect and mediated by integrin-linked kinase (ILK)–PINCH–Parvin complex (Honda et al., 2013). ILK binds directly to K2

*K. Bledzka and K. Bialkowska contributed equally to this paper.

Correspondence to Edward F. Plow: plowe@ccf.org; or Jun Qin: qinj@ccf.org

Abbreviations used in this paper: ABS, actin binding site; FA, focal adhesion; ILK, integrin-linked kinase; MFI, mean fluorescence intensity; NT, nontargeting; SPR, surface plasmon resonance.

The Rockefeller University Press $30.00
J. Cell Biol. Vol. 213 No. 1 97–108
www.jcb.org/cgi/doi/10.1083/jcb.201501006

(Tu et al., 2001; Qadota et al., 2012), and Parvin links to other FA components (Schaller, 2001). In the present study, we provide evidence for direct interaction of K2 with actin and demonstrate that an ABS resides in its F0 domain. This ABS influences cell spreading, thereby defining a new mechanism for K2 to participate in integrin signaling.

Results

Kindlins, including K2, colocalize with actin in FA and related structures as shown by immunofluorescence (Tu et al., 2003; Shi et al., 2007; He et al., 2011; Qu et al., 2011). However, direct interaction of K2 with actin has not been reported. In staining actin in MAE cells from *kindlin-2*$^{+/-}$ mice, we noted marked disorganization of actin filaments compared with those in wild-type (WT) MAE cells (Fig. 1 A) when spread on vitronectin; the MAE cells from *kindlin-2*$^{+/-}$ mice lacked stress fibers and were less well spread. This difference was not evident when the MAE cells were spread on fibronectin (Fig. 1 B). Quantification of cell areas (Fig. 1 C) verified that the differences in spreading of *kindlin-2*$^{+/-}$ MAE cells versus WT endothelial cells on vitronectin was very significant ($P < 0.001$), but spreading on fibronectin was not ($P > 0.5$). The preferential decrease in adhesion to vitronectin compared with fibronectin was not caused by a decrease in expression of the primary vitronectin receptor, αVβ3, on endothelial cells. We previously reported that β3 expression levels detected by flow cytometry on WT and *kindlin-2*$^{+/-}$ MAE cells were very similar (Pluskota et al., 2011). Moreover, although the binding of a soluble ligand, fibrinogen, to αVβ3 was markedly suppressed when the *kindlin-2*$^{+/-}$ MAE cells were stimulated with VEGF compared with WT MAE cells, when the two cell types were treated with Mn^{2+}, an external integrin activator, they bound similar levels of fibrinogen (Pluskota et al., 2011). Our results are also consistent with the study by Liao et al. (2015) demonstrating the importance of K2 in αVβ3-mediated responses.

To assess whether K2 is important for actin organization in a second cell type, we used mouse C2C12 cells, a widely used line for myogenic differentiation studies (Janot et al., 2009). C2C12 cells express only K2, but not K1 or K3 (Dowling et al., 2008b). K2 localizes in FA and along actin stress fibers in C2C12 cells (Fig. 1 D). With siRNA, >90% knockdown of K2 was attained at 24 h as assessed by Western blot, whereas expression of control FA proteins (FAK, viculin, and β1 integrin) was similar (Fig. S1 A), and surface expression of β1 integrins was also not reduced as assessed by flow cytometry (Fig. S1 B). However, actin organization was markedly different in the two cell types (Fig. 1 E): in the cells treated with K2 siRNA, actin was located only at the cell periphery and actin stress fibers were absent. Cell area, measured at 1 h after spreading on fibronectin, was significantly ($P < 0.001$) reduced by K2 knockdown (Fig. 1 F).

A previous study suggested that knockdown of K2 in C2C12 cells that were undergoing differentiation in myotubes induced by serum starvation altered distribution of ILK and FA (Dowling et al., 2008b). To assess whether K2 siRNA knockdown in the undifferentiated C2C12 cells adherent to fibronectin could also alter their FA formation and ILK distribution, we detected FA by anti-vinculin staining and ILK distribution by transfecting the cells with EGFP-ILK (Fig. S2 A). As noted in Fig. 1 (D–F), C2C12 cells with K2 knocked down spread less well on fibronectin, and consequently fewer cells exhibited FA. However, in the spread cells, the FA marked by vinculin staining still contained ILK (Fig. S2 B). The ILK staining tended to be peripherally located (Fig. S2 B), consistent with the membrane localization of ILK when K2 was knocked down in differentiated C2C12 cells as noted by Dowling et al. (2008b).

Our observations relating K2 to actin organization in MAE and C2C12 cells led us to explore the direct interaction between K2 and actin. For these studies, purified K2 was needed. Full-length K2 was expressed in *Escherichia coli* as a GST fusion protein and purified on glutathione-Sepharose, as previously published (Bledzka et al., 2010, 2012). GST tag was removed from K2 by Factor Xa cleavage. K2 prepared in this way was homogeneous by SDS-PAGE and showed little evidence of aggregation by gel filtration (Fig. 2 A). The purified K2 was then assessed for interaction with actin using commercial protein spin-down assay kits. K2 was added to F-actin; BSA was used as a negative control, and α-actinin, a known actin-binding protein, as a positive control. After 30 min, pellets and supernatants were separated by centrifugation and analyzed by SDS-PAGE (Fig. 2 B). As determined by densitometric scanning of the gel, only 2% of the added BSA cosedimented with actin, whereas 52% of the added α-actinin associated with actin (Fig. 2 B). A significant proportion, 36%, of the added K2 associated with the actin pellet. From three similar experiments, the percentage of added K2 that associated with the actin ranged from 30% to 54%.

Next, we measured the direct binding of purified K2 to actin by surface plasmon resonance (SPR). Various concentrations of K2 were allowed to flow over F-actin immobilized by amine coupling onto CM-5 biosensor chips. Time- and concentration-dependent binding of K2 followed by a dissociation phase was observed (Fig. 3 A). The progress curves shown in Fig. 3 A were derived by subtracting the customary controls for bulk effects of solvent and for K2 binding to blank chips using the instrument's BIAevaluation software. Representative binding curves of K2 interaction with the actin-coated chips, with and without these corrections, are shown in Fig. S3. Additionally, as controls for specificity, K2 binding to other immobilized proteins, BSA (Fig. 3 B) or myosin (Fig. 3 C), were tested, and minimal binding was detected. All control proteins were immobilized at the same coating density as actin. To consider whether the observed binding was caused by some residual GST tag in the K2 preparations, we tested GST binding to the actin-coated biosensor chips, but no interaction was detected (Fig. 3 D). We also tested whether K2 bound exclusively to F-actin. An actin mutant that is unable to polymerize and thereby mimics G-actin (Joel et al., 2004) was coated onto the biosensor chips. The various concentrations of K2 bound to this G-actin mimetic (Fig. 3 E) in a manner similar to their interaction with F-actin (Fig. 3 A). In interpreting the SPR progress curves in Fig. 3, A and E, with BIAevaluation software, we noted that those that generated a lower concentrations of K2 (<1 µM) conformed to a 1:1 Langmuir model with χ^2 (an estimate of goodness of fit) values of less than five, whereas data generated at higher K2 concentrations did not fit this model well or any models within the instrument's software package (χ^2 values of ≥20). The estimated K_d determined from the SPR curves at the lower K2 concentrations (χ^2 values of less than five) yielded values of the two actins for K2 of 1.36×10^{-7} M for F-actin and 1.24×10^{-7} M for G-actin mutant.

A major ABS resides in the F0 domain of K2

To locate an ABS within K2, we compared its sequence to known actin-binding proteins in the database of eukaryotic linear

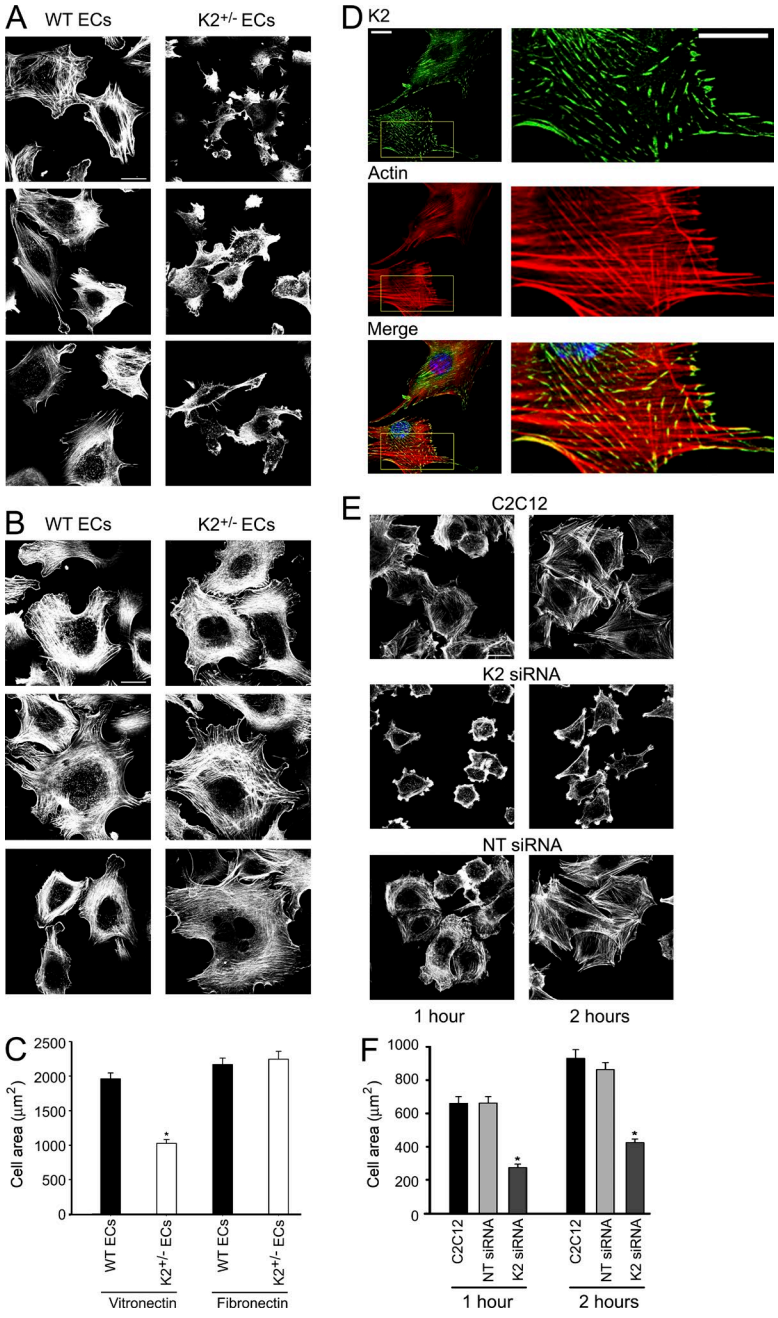

Figure 1. **Actin disorganization in cells expressing reduced K2.** (A and B) Visualization of actin in MAE cells (ECs) from WT and $K2^{+/-}$ mice. MAE cells were spread on vitronectin (A) or fibronectin (B) for 2 h, fixed, and stained with Alexa Fluor 488–phalloidin. Bar, 20 µm. (C) Areas of cells were measured using ImageJ software, and 80 cells were quantified in each sample. The error bars represent means ± standard error of two independent experiments (*, $P < 0.001$ vs. WT endothelial cells [control] by Student's *t* test.). (D) Visualization of actin and K2 in C2C12 mouse myoblastoid cells. K2 (green) colocalized with actin (red) in filaments and FA. The merged image of K2 (green) with actin (red) is shown in the bottom panel. The C2C12 cells were spread on fibronectin for 1 h, fixed, permeabilized, and stained with anti-K2 followed by Alexa Fluor 488 anti-mouse IgG and Alexa Fluor 568–phalloidin. Bar, 10 µm. Higher-magnification images to visualize actin stress fibers are shown next to each panel. Bar, 5 µm. (E) Visualization of actin in C2C12 cells after K2 knock-down with siRNA. C2C12 cells were spread on fibronectin for 1 or 2 h, fixed, and stained with Alexa Fluor 488–phalloidin. F-actin is in a linear pattern in untreated cells (top) and cells treated with NT-siRNA (bottom) but redistributes to the membrane in cells treated with K2 siRNA (middle). Bar, 20 µm. (F) Areas of cells were measured using ImageJ software, and 100 cells were quantified in each sample. Means ± standard error of two independent experiments are shown (*, $P < 0.001$ vs. C2C12 control by Student's *t* test).

motifs. Two overlapping ABSs, K2(20–36) and K2(32–49), within the K2F0 domain were predicted. To test this prediction, two K2 fragments, K2(1–105) containing F0 and K2(281–541) containing F2, were expressed in *E. coli* as GST fusion proteins, purified, and used in GST pull-down assays. The K2F0 fragment interacted with actin, whereas the K2F2 fragment failed to pull down actin (Fig. 4 A). We then expressed K2F0 and two mutant K2F0 fragments, each with a double mutation at surface residues, K2F0($E^{38}A/H^{40}A$) or K2F0(LK^{47}/AA), based on the solution structure of K2F0 (Perera et al., 2011). In GST pull-down assays, K2F0 and the K2F0($E^{38}A/H^{40}A$) mutant interacted with actin, whereas the K2F0(LK^{47}/AA) mutant and the GST control protein failed to interact (Fig. 4 B). To confirm this localization, we expressed WT K2 or a $K2LK^{47}/AA$ mutant and used these in GST pull-down experiments (Fig. 4 C). WT K2 pulled down substantially more actin compared with $K2LK^{47}/AA$. Based on densitometric scans of the intensities of the actin bands from six experiments with two different WT and mutant K2 preparations, the K2 mutant pulled down 54–99% less actin than the WT K2, with a mean reduction of 75%. Note that in the experiments shown in Fig. 4, K2 and its fragments showed a consistent ability to interact with actin, regardless of whether they were presented in the lysates of different human cells or as purified from rabbit skeletal muscle. Both WT K2 and $K2LK^{47}/AA$ interacted with ILK in GST pull-down experiments (Fig. 4 D). This reactivity is consistent with the location of the ILK binding site in the F2 subdomain of K2, distinct from the ABS in F0 (Huet-Calderwood et al., 2014; Fukuda et al., 2014).

The interaction of WT and the $K2LK^{47}/AA$ mutant were compared in SPR experiments. At all concentrations tested (0.1–3 µM), the progress curves of mutant K2 showed lower binding than those of WT K2 (Fig. 5, A and B). These binding

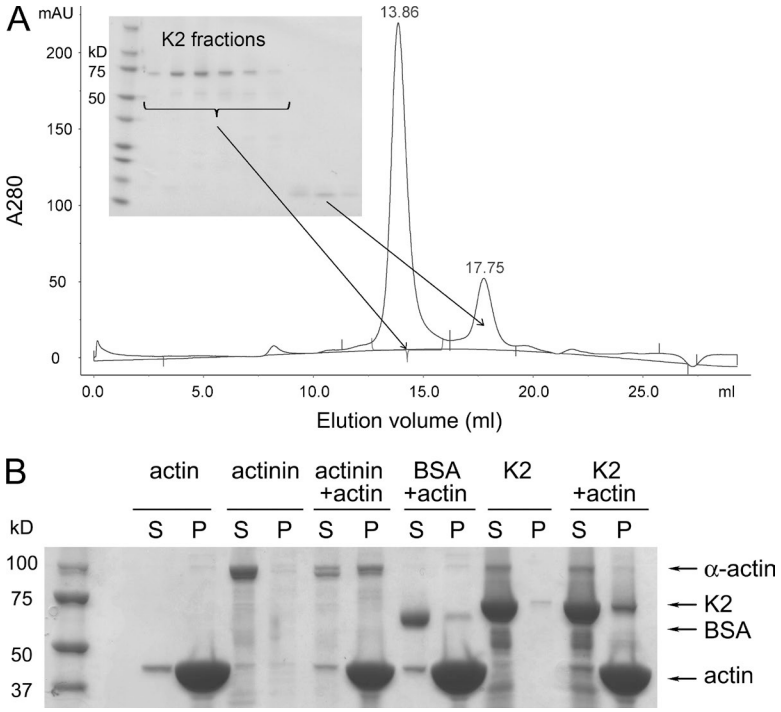

Figure 2. **K2 purification and direct binding to actin.** (A) Superdex 200 10/300 GF column elution profile of K2 (75 kD). K2 after GST-Sepharose purification and GST cleavage with Factor Xa was subjected to gel filtration on a Superdex 200 10/300 GL. Protein was eluted with 20 mM Tris, 100 mM NaCl, and 1 mM DTT, pH 8.0, at a flow rate of 0.5 ml/min. The void volume was ∼8 ml, the bed volume was 24 ml, and the elution volume for BSA (66 kD) under the same conditions was ∼14 ml. SDS-PAGE of peak fractions is shown as an inset. mAU, milli–arbitrary unit. (B) Association of K2 with actin by cosedimentation. K2, BSA, or α-actinin, each at 10 µM, was added to F-actin and incubated for 30 min, and supernatant (S) and pellet fractions (P) were separated by centrifugation and analyzed by SDS-PAGE (4–20% gel).

studies were all performed in the same experiment, and all samples were analyzed on the same sensor chip but are separated into two panels to more readily display the curves obtained at the same concentrations of WT and mutant K2 (Fig. 5, A and B). As noted earlier, analysis of the kinetic data at all concentrations of K2 tested did not conform well to a 1:1 Langmuir binding model, as reflected by large deviations from the goodness-of-fit parameter, χ^2. This was also the case with the K2LK^{47}/AA mutant. Indeed, when all concentrations of WT K2 or K2LK^{47}/AA were considered, the binding curves did not fit well to any of several models available in the BIAevaluation software. From the lower concentrations of WT K2 and K2LK^{47}/AA mutant, we estimated their K_d values for actin at $1.36 \pm 0.24 \times 10^{-7}$ and $15.8 \pm 3.4 \times 10^{-7}$ M, respectively. In an effort to estimate the binding affinities of WT and K2LK^{47}/AA mutant for actin, we used a steady-state method. Representative SPR curves for WT and mutant K2 are shown in Fig. 5 (A and B). Data from two independent experiments in which the maximum

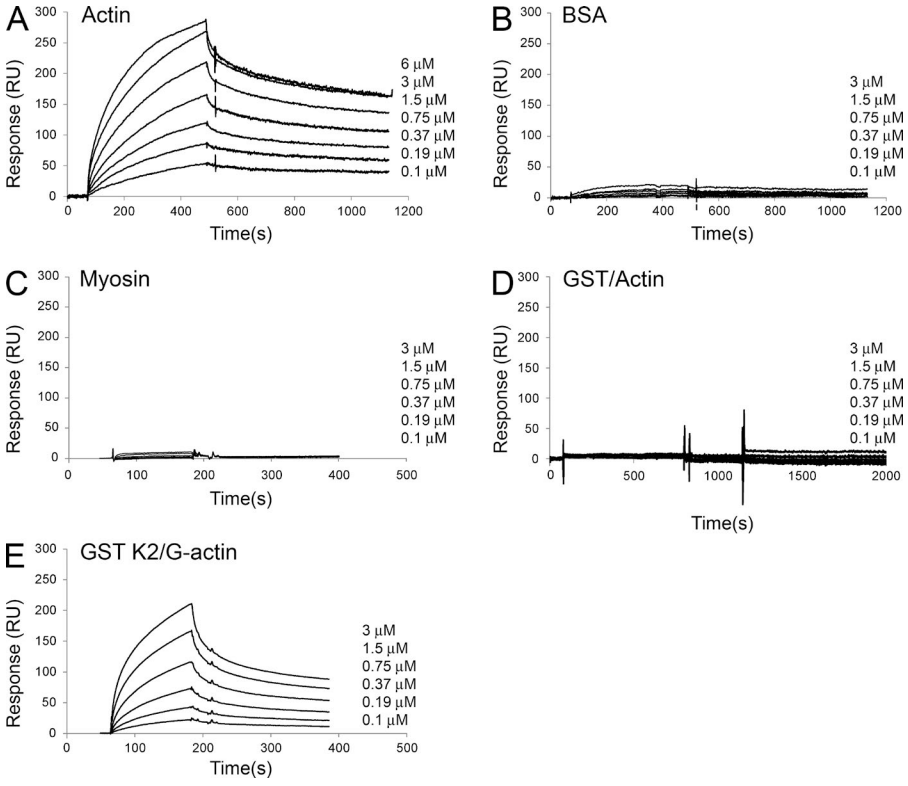

Figure 3. **Binding of K2 to actin by SPR.** (A) Actin was immobilized on CM5 biosensor chips. Various concentrations of full-length K2 (GST constructs) was injected over the coated chips, and the progress curves of binding were recorded. (B and C) The experimental conditions are the same as in A except that the CM5 biosensor chips were coated with BSA (B) or myosin (C). (D) Chips were coated with actin as in A, but the soluble analyte was GST alone. (E) Conditions are the same as in A except that the biosensor chip was coated with an actin mutant (Joel et al., 2004) that cannot polymerize, a mimetic of G-actin. The coating densities of all proteins on the chips were similar based on response unit (RU) values of ∼1,000. The progress curves shown have had mock runs (buffer only) and the empty flow cell controls subtracted. Tracings of K2 binding to actin are representative of at least eight experiments.

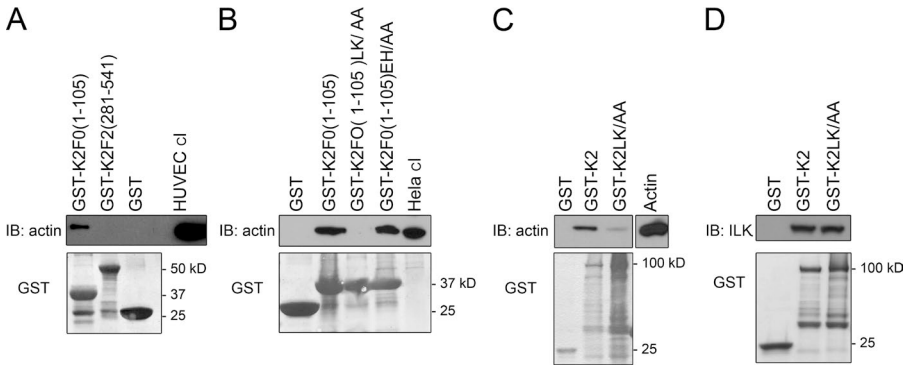

Figure 4. **LK[47] residues in the F0 domain of K2 are essential for actin binding.** (A) GST-fused K2, a GST-K2F0 fragment, a GST-K2F2 fragment, and GST alone were added to the lysates of HUVECs followed by 20 µl glutathione-Sepharose 4B. The bound actin was measured by immunoblotting (IB) with an anti-actin antibody. (B) GST-fused K2, a GST-K2F0(1–105) fragment, GST-K2F0(1–105) LK[47]/AA mutant, GST-K2F0(1–105)E[38]H[40]/AA, and GST alone were used in pull-down assays to precipitate actin from HeLa cell lysates as in A. (C) GST-fused K2, GST-K2LK[47]/AA mutant, and GST alone were used in pull-down assays to precipitate actin purified from rabbit skeletal muscle. (D) GST-fused K2, GST-K2LK[47]/AA mutant, and GST alone were used in pull-down assays to precipitate ILK from HeLa cell lysates as in A. Below each panel is the loading control. The gels below A, B, and C are stained with Amido black and that below D with Coomassie blue.

response signals were measured are plotted versus concentration in Fig. 5 C. These plots indicated that binding of both WT and mutant K2 approached saturation. These data yielded estimated K_d values of $1.90 \pm 0.55 \times 10^{-7}$ M for WT K2 and $9.82 \pm 0.40 \times 10^{-7}$ M for K2LK[47]/AA. Although the ~5-fold difference in values using the same technique is valuable for comparison, because of the complexities of the binding curves, we consider these to be relative K_d values. We also implemented an approach unrelated to SPR. Actin was coated onto microtiter plates, and K2 binding was quantified using an anti-GST and secondary HRP-labeled IgG. From the binding isotherms generated, the relative K_d values of WT and mutant K2 differed by three- to fivefold. Two such experiments were performed, each with duplicate or triplicate determinations at eight to nine different K2 concentrations. One of these experiments is shown in Fig. S4.

We next tested whether WT K2 and K2LK[47]/AA differed in their capacity to induce actin reorganization. For these experiments, the K2 forms with GST tags removed were used and were allowed to polymerize with actin for 60 min. The samples were diluted into buffer containing Alexa Fluor 488–phalloidin, applied to a coverslip coated with poly-L-lysine, and, after 60 min, visualized by fluorescence microscopy. In the absence of K2, Alexa Fluor 488–phalloidin–labeled actin formed a uniform carpet of fine filaments (Fig. 6). At 1 µM, α-actinin, a known actin-bundling protein, induced formation of spider-like aggregates with radiating filaments. At 1 µM, WT K2 also reorganized actin, with clumps and filaments both observed. In contrast, the carpet of actin showed minimal perturbation by K2LK[47]/AA at the same concentration (1 µM) as WT K2. At a higher concentration (6 µM), K2LK[47]/AA did induce a weak aggregation of actin (Fig. 6). These data not only support the interaction of K2 with actin but also ascribe a functional outcome, actin reorganization, to this interaction. Mutation of only two residues in the ABS in F0 diminishes this functional activity.

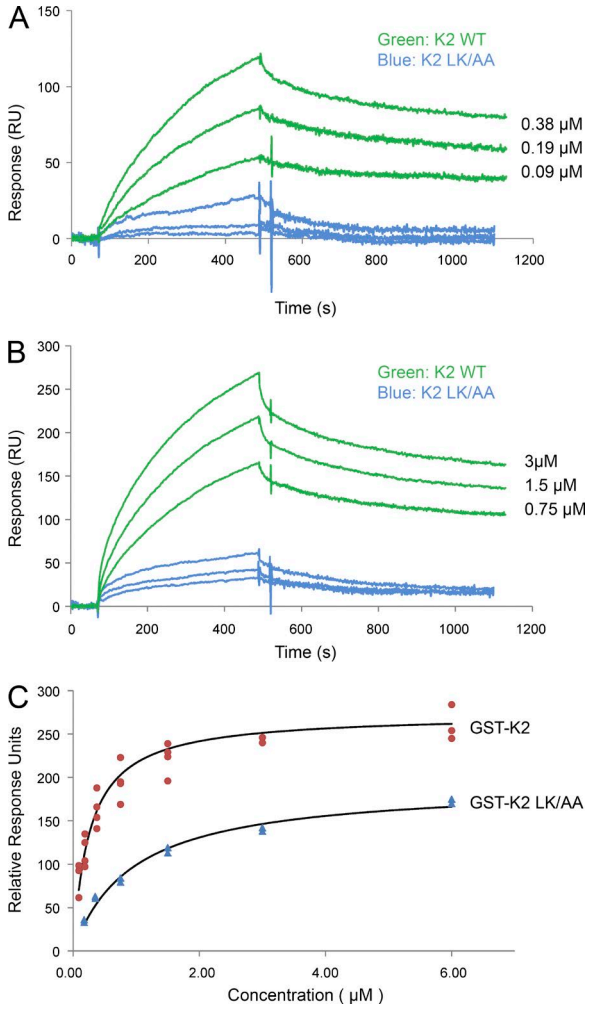

Figure 5. **Effect of the LK[47]/AA mutation in K2 on direct actin binding by SPR.** (A and B) SPR tracings comparing the binding of WT GST-K2 and mutant K2 (GST-K2LK[47]/AA) to actin immobilized on a CM5 biosensor chip. Lower concentrations of the K2 forms are shown in A and higher concentrations in B. (C) Steady-state binding curves for GST-K2 and GST-K2LK[47]/AA. Steady-state responses at the end of the association phase were used to determine $K_{0.5}$. Data points are averages from duplicate runs from two independent experiments. RU, response unit.

Role of theABS in F0 in inside-out and outside-in signaling

To evaluate the contribution of the ABS in K2F0 in inside-out signaling, we used a well-established integrin coactivation assay (Ma et al., 2008). Coexpression of DsRed–talin-H and EGFP-K2 in CHO-A5 cells resulted in a significant increase in binding of PAC-1, a mAb that reports on the activation status of αIIbβ3

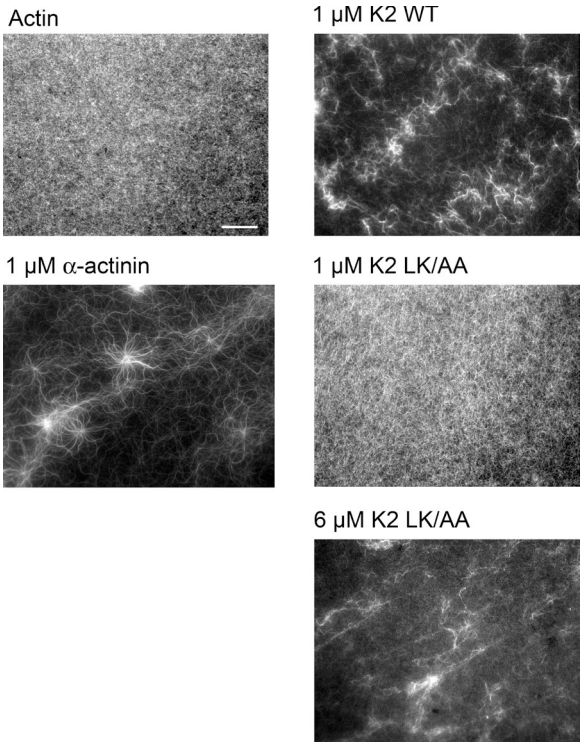

Figure 6. **The effect of K2 on actin filaments is visualized by Alexa Fluor 488–phalloidin staining.** Actin was allowed to polymerize in the absence of K2 (negative control), in the presence of 1 µM α-actinin, a known actin bundling protein, or in the presence of K2 at 1 µM and K2LK^{47}/AA at 1 and 6 µM. K2 forms used in these experiments had GST tag removed.

(Shattil et al., 1987). Coactivation of the integrin is induced by K2 plus talin-H compared with talin-H alone (Fig. 7 A). K2QW^{615}/AA mutant, which blunts integrin binding (Ma et al., 2008; Xu et al., 2014), lost the ability to support coactivation of αIIbβ3. However, the K2LK^{47}/AA exhibited coactivation activity similar to that of WT K2 (Fig. 7 A). Thus, the ABS activity in K2F0 is not required for the integrin coactivating function of K2.

Further evidence that the K2L^{47}/AA mutation exerted its effect on outside-in and not inside-out integrin signaling was derived from experiments performed with C2C12 cells in the presence of Mn^{2+}, which induces activation of the extracellular ligand binding site within integrins. The C2C12 cells were treated with nontargeting (NT) siRNA or K2 siRNA or were untreated for 24 h; they were then spread on fibronectin for 30 min in the presence of Mn^{2+}. Mn^{2+} supported rapid spreading of the cells whether treated with NT or K2 siRNA, indicative of activation of the integrins by Mn^{2+} treatment. However, as noted from the gallery of micrographs displayed in Fig. 7 B, the cells treated with K2 siRNA were less well spread and remained smaller, and their actin was less well organized. The actin disorganization and spreading defect associated with K2 knockdown in the presence of Mn^{2+} was similar to that seen with these same cells in the absence of Mn^{2+} at 1 or 2 h in Fig. 1 E. Quantitation of C2C12 cell spreading in the presence of Mn^{2+} at 30 min (Fig. 7 C) indicated that K2 knockdown diminished their size by ∼60%. Note that the size of the C2C12 cells in the presence of Mn^{2+} at 30 min was about the same as attained at 2 h in the absence of Mn^{2+} (Fig. 1 F, right, in the presence of Ca^{2+} + Mg^{2+} alone), verifying that Mn^{2+} had a marked effect on cell spreading, indicative of integrin activation.

To test the role of the ABS in K2F0 on integrin outside-in signaling, we examined the capacity of WT K2 and K2LK^{47}/AA to support C2C12 cell spreading. Verifying the results in Fig. 1 (E and F), knockdown of K2 inhibited spreading of these cells. The K2 siRNA used in these knockdown experiments targeted a sequence in the 3′ UTR of K2, allowing for expression of K2 variant proteins in these cells. Expression of WT K2 in the knockdown cells "rescues" spreading (representative micrographs in Fig. 8 A). In contrast, expression of K2LK^{47}/AA in the cells failed to rescue the spreading defect in the cells (Fig. 8 B). Quantitation of the spreading of these cells at 1 or 2 h after spreading on fibronectin showed that WT K2 rescued the cells but the K2LK^{47}/AA mutant did not (Fig. 8 C). Fig. S5

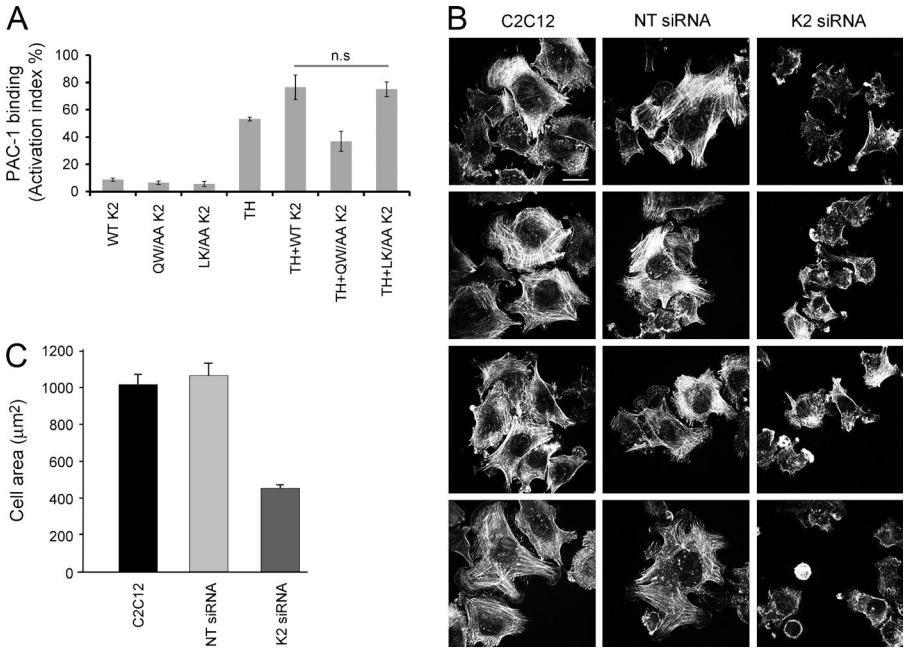

Figure 7. **Effect of the LK^{47}/AA mutation in K2 on integrin inside-out signaling.** (A) Role of the ABS in F0 in inside-out signaling. CHO-A5 cells stably expressing integrin αIIbβ3 were in transfected with EGFP constructs for full-length WT K2 (E-K2), K2(LK^{47}/AA) mutant, which diminishes its ABS in F0, or K2(QW^{615}/AA) mutant, which diminishes its integrin-binding function (Ma et al., 2008). These K2 constructs were cotransfected with talin-H (TH), and integrin activation was quantified by flow cytometry based on PAC-1 binding, an antibody specific for activated αIIbβ3 (Shattil et al., 1985). Changes in integrin expression level were excluded with a mAb that reacts equally with the resting and active integrin. Data represent means ± SD of three independent experiments. n.s., not significant. (B) Visualization of actin in C2C12 cells after K2 knock-down with siRNA. C2C12 cells were spread on fibronectin in the presence of 3.5 mM $MnCl_2$ for 30 min, fixed, and stained with Alexa Fluor 488–phalloidin. Bar, 20 µm. (C) Areas of cells were measured using ImageJ software, and 60 cells were quantified in each sample.

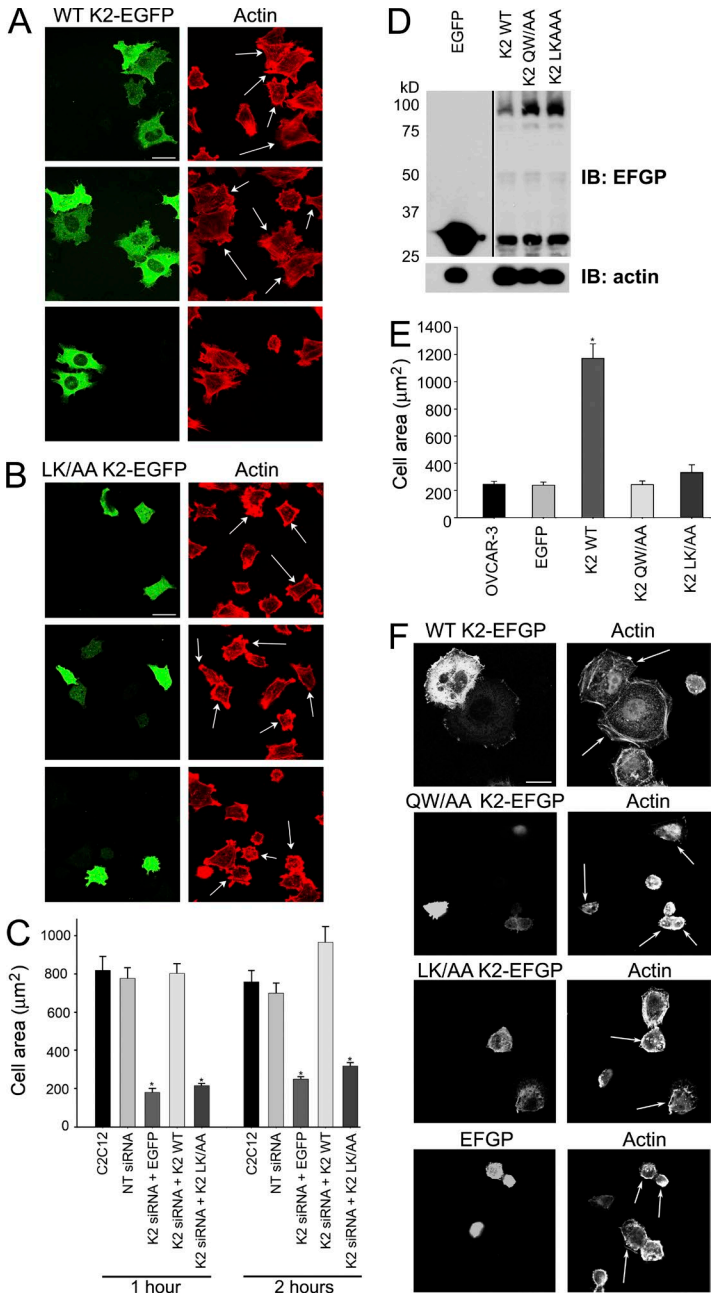

Figure 8. **Effect of the LK[47]/AA mutation in K2 on integrin outside-in signaling.** (A) Visualization of actin in C2C12 cells after K2 knock-down and rescue with EGFP-tagged WT K2. C2C12 cells were spread on fibronectin for 1 h, fixed, and stained with Alexa Fluor 568–phalloidin. Transfected cells were visualized with EGFP fluorescence. Transfected cells in righthand panels are identified with arrows. Bar, 20 µm. (B) Visualization of actin in C2C12 cells after K2 knock-down cotransfection with EGFP-tagged LK/AA K2 mutant. C2C12 cells were spread on fibronectin for 1 h, fixed, and stained with Alexa Fluor 568–phalloidin. Transfected cells were visualized with EGFP fluorescence. Transfected cells in righthand panels are indicated with arrows. Bar, 20 µm. (C) Quantitative analysis of C2C12 cell spreading coexpressing siRNA and EGFP-tagged K2 constructs. C2C12 cells were spread on fibronectin for 1 or 2 h, fixed, and stained with Alexa Fluor 568–phalloidin. The areas of EGFP-positive cells were measured using ImageJ software. *, $P \leq 0.001$ vs. C2C12 control by Student's *t* test. 40–50 cells were quantified in each sample from two independent experiments. (D) Western blot showing levels of expression of EGFP-tagged K2 constructs in OVCAR-3 cells. The blots were probed with anti-EGFP antibody and anti–β actin antibody as a loading control. EGFP alone was expressed at much higher levels than any K2 construct, and a lower exposure is shown for the EGFP blot (separated by the vertical line). (E) Quantitative analysis of OVCAR-3 cell spreading overexpressing WT K2 (E-K2), K2(LK[47]/AA), or K2(QW[615]/AA). OVCAR-3 cells were spread on 20 µg/ml fibronectin for 1 h, fixed, and stained with Alexa Fluor 633–phalloidin. Areas of EGFP-positive cells were measured using ImageJ software. *, $P \leq 0.001$ vs. OVCAR-3 by Student's *t* test. 40–50 cells were quantified in each sample in two independent experiments. (F) Actin organization in OVCAR-3 cells expressing K2 proteins. Cells were spread on fibronectin as described in F, and transfected cells were identified with EGFP fluorescence. Transfected cells are indicated with arrows in righthand panels. Bar, 20 µm.

A verifies that the expression levels of the K2 mutants in the transfected cells were not less than WT K2.

C2C12 cells were evaluated to determine whether K2LK[47]/AA could still be recruited into FA. C2C12 cells were K2 knocked down and rescued with the EGFP-K2LK[47]/AA mutant, were allowed to adhere to fibronectin for 2 h, and were costained with antibodies to viculin as an FA marker. Although few cells expressing the K2LK[47]/AA spread, those that did had FA positive for EGFP-K2LK[47]/AA; costaining with anti-viculin verified that it was present in FA (Fig. S5 B). We also used C2C12 cells to test whether expression of the K2LK[47]/AA mutant would suppress the function of endogenous K2. C2C12 cells were transfected with the EGFP vector alone or with EGFP-tagged K2LK[47]/AA mutant. After 24 h, the cells were spread for 1 h on fibronectin in the presence of Ca^{2+} and Mg^{2+}. We measured the area of 65 phalloidin-stained cells: untransfected cells, 609.4 ± 20.6 µm^2; EGFP$^+$ cells, 646.3 ± 24.7 µm^2; and K2LK[47]/AA-transfected cells, 382 ± 20.5 µm^2 (unpublished data). The difference between the EGFP$^+$ and K2LK[47]/AA mutant-expressing cells was significant ($P = 0.001$).

OVCAR-3 is an ovarian cancer cell line in which several chromosomes, including chromosome 14 where K2 resides, are underrepresented (Hamilton et al., 1983). Western blots of OVCAR-3 cell lysates verified the absence of K2 and the presence of only low levels of kindlin-1 and kindlin-3 (relative to BT549 cells, a triple-negative breast cancer cell line) in these cells (Fig. S5 C). The absence of K2 in these cells by Western blot confirms our previously published data (Fukuda et al., 2014). These cells express β1 integrin as assessed by flow cytometry, and their spreading was assessed on fibronectin 1 h after transfection with WT K2, mutant K2, or K2(QW[615]/AA). The similar expression of the K2 proteins in the transfected cells was verified by Western blot (Fig. 8 D). Parental OVCAR-3 cells and EGFP-transfected cells exhibited limited spreading on fibronectin

(Fig. 8 F). WT K2 enhanced cell spreading by greater than fourfold, whereas the K2 mutant enhanced spreading only modestly. Transfection of OVCAR cells with K2(QW^{615}/AA) also failed to support cell spreading (Fig. 8 E). Moreover, in staining actin in parental OVCAR-3 cells and cells expressing EGFP and the K2 mutant, we noted marked absence of well-organized actin filaments (Fig. 8 F, transfected cells indicated with arrows) compared with those transfected with WT K2, which spread and developed well-organized stress fibers (Fig. 8 F).

Discussion

The present study has demonstrated that K2 is an actin-binding protein. This finding assigns a new function to K2 and appears to contribute at least in part to the disorganization of actin filaments and decreased spreading observed in MAE cells derived from *kindlin-2*$^{+/-}$ mice and C2C12 myoblastoid cells, in which K2 levels were reduced by siRNA treatment. The actin-binding activity of K2 is also consistent with the actin disorganization in *kindlin-2*$^{-/-}$ embryoid bodies, which show basolateral accumulation of F-actin instead of the characteristic apical F-actin belt (Montanez et al., 2008), and the pronounced muscle cell rounding in *Caenorhabditis elegans* with null mutation of UNC-112, the orthologue of K2 (Rogalski et al., 2000). These profound effects may not depend exclusively on the actin-binding activity of K2, but the ABS in F0 that we have identified may contribute to these phenotypes.

Several independent approaches—cosedimentation, coimmunoprecipitation, SPR, and actin-bundling experiments—all pointed to a direct interaction of K2 with actin. Analysis of the primary amino acid sequence to a database (Dinkel et al., 2014) of known actin-binding motifs led to the prediction of ABS activity within the F0 subdomain. Of two overlapping ABSs predicted in F0, mutational analyses identified the one centering around LK^{47} as implicated in actin binding. Mutations of LK^{47} to alanines reduced the actin-binding activity of F0 and intact K2 in coimmunoprecipitation, GST pull-down, actin-bundling, and SPR experiments. F0 assumes a ubiquitin-like fold (Perera et al., 2011). K2LK^{47} resides in a short helix (Fig. 9 A) extending from G^{31}-K^{51}, and ABSs are often harbored in short helices containing LK sequences (Friederich et al., 1992; Vardar et al., 1999). The face of F0 in which this helix resides is spatially distant from the charged face composed of H^{40}/K^{74}/H^{76}/W^{77}/K^{81}, which forms a phospholipid binding motif that helps target K2 to membranes (Perera et al., 2011). Of note, LK^{47}, as well as many adjacent residues, is very highly conserved in K1 and K3 (Fig. 9 B), suggesting that actin binding may be a common function of F0 domains among the kindlins.

K2 binding to immobilized actin in SPR studies deserves special comment. These experiments clearly showed that K2 binds to actin but not to control proteins. However, the SPR progress curves showed some deviations from ideal behavior, including failure to saturate at the highest testable concentrations of K2, incomplete dissociation kinetics, and failure to conform to a simple 1:1 binding model. The complexity of the SPR data probably arises in part from the actin substrate and in part from the properties of K2. Roman et al. (2006) reported that protein binding to actin can present some unusual behavior in SPR experiments in analyzing VDAC binding to actin. With regard to K2, K2 tends to self-associate (Qadota et al., 2012), and this behavior may contribute to the failure to saturate actin

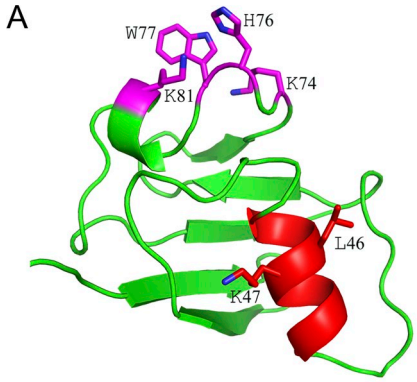

Figure 9. **Model of ABS in K2.** (A) Ribbon diagram displaying the previously determined solution structure of K2 F0 (Perera et al., 2011). The LK^{47} residues within the ABS reside in a helix that extends from residues 31–51 that is colored in red. The residues that compose the previously identified charged phospholipid-binding interface are in blue. (B) Alignment of the actin-binding region in the F0 region of K2 with the corresponding regions of kindlin-1 and kindlin-3. LK^{47} has been boxed in all kindlins.

at higher K2 concentrations. Such self-association is observed for other ERM proteins and can influence their interactions with actin (Turunen et al., 1994; Gary and Bretscher, 1995; Zhu et al., 2008). Despite these complexities, the SPR data are valuable; they establish that K2 binds specifically and directly to actin (Fig. 5) and that the LK^{47}/AA K2 mutant binds less well to actin than WT K2 under the same conditions (Fig. 5). The fivefold difference in the relative affinity of WT and mutant K2 for actin was consistent with two approaches to analyze the SPR data and consistent with the differences in their activities in pull-down and actin-bundling experiments. K2 also appears to bind to G-actin. An actin mutant that is unable to polymerize and thereby mimics G-actin (Joel et al., 2004) was coated onto the biosensor chips and used in SPR experiments. The various concentrations of K2 bound to this G-actin mimetic (Fig. 3 E) in a manner similar to their interaction with F-actin (Fig. 3 A). This observation leads to the prediction that changes in the polymeric state and location of F- and G-actin during cellular responses could change the distribution of kindlins within cells.

We believe that K2 may have at least one additional ABS. Evidence for an additional ABS in K2 comes from experiments showing that the LK^{47}/AA mutant retains some actin-binding activity in pull-down, SPR (Figs. 4 and 5), and actin-bundling (Fig. 6) experiments. Indeed, preliminary alignment of the sequence of K2 with known actin-binding proteins predicts an additional ABS in F3. Of note, this ABS would be absent in K2F2, and we show that K2F2 does not bind actin under conditions where K2F0 binds well (Fig. 4 A). The localization of such additional ABSs and whether they operate independently of or are part of the F0 ABS is beyond the scope of the present article. In either case, such an ABS would still contribute to the residual affinity of the LK/AA mutant for actin. Moreover, the contribution of such hypothetical ABSs to function need not be proportional to their contribution to the affinity of K2 for actin.

Clearly, the ABS that we identify in K2F0 is functionally important (Fig. 8). The actin aggregates induced by WT K2

were not identical to the actin bundles induced by α-actinin, but such differences are often noted among various actin-binding proteins and are dependent on the conditions and concentrations of the actin-bundling proteins (Tseng et al., 2004). Whether the aggregates formed in the presence of K2 represent true actin bundles will require further analyses. It has been suggested that the role of kindlins in integrin activation depends on its clustering of integrins (Ye et al., 2013). Actin binding by K2 would provide a mechanism to achieve such clustering. However, we found no evidence that the ABS in F0 influences integrin coactivation in the widely used αIIbβ3-CHO cell assay. Also, the defect in C2C12 cell spreading with K2 knockdown was not overcome when integrins were activated with Mn^{2+}, indicating that the spreading defect was not secondary to an activation defect. In contrast, our data provide clear evidence that the ABS in the F0 subdomain of K2 does influence integrin outside-in signaling. The defect in spreading of C2C12 myoblastoid cells caused by siRNA knockdown of K2 was restored by transfection with an expression vector encoding a siRNA-resistant WT K2 but not with one encoding the LK^{47}/AA mutant. $K2LK^{47}$/AA, when overexpressed in C2C12 cells, overcame the effect of endogenous K2 and caused a spreading defect, illustrating the general importance of this ABS to the cell-spreading functions mediated by K2. The few C2C12 cells expressing $K2LK^{47}$/AA that were able to spread on fibronectin did display FA. When K2 was knocked down in myotube-like structures formed by serum-starved C2C12 cells, Dowling et al. (2008b) reported that the FAs were irregular and ILK was associated with the cell membrane. In our undifferentiated C2C12 cells with K2 knockdown, ILK was associated with FA but tended to be more peripherally located than in cells without K2 knockdown. Whether these differences reflect retention of some functions of K2 by the $K2LK^{47}$/AA mutant or the unique functions of K2 in the myotube-like cells is uncertain. In OVCAR cells that have negligible levels of endogenous K2, expression of WT K2, but not $K2LK^{47}$/AA, enhanced cell spreading. Low levels of K1 and K3 were detected in OVCAR cell lysates by Western blot, but the endogenous levels of the kindlins were not sufficient to support the robust spreading of these cells when transfected to express WT K2. The inability of another kindlin to substitute for K2 has been noted in other cell types (Bialkowska et al., 2010; Bandyopadhyay et al., 2012; Rozario et al., 2014).

In sum, our studies identify K2 as an actin-binding protein. An ABS located in F0 influences outside-in signaling across integrins. These findings provide the underpinnings for considering new roles of kindlins in integrin and more broadly in cell biology.

Materials and methods

Antibodies and reagents

The following primary antibodies were used: PAC1, which reacts selectively with the activated conformation of integrin αIIbβ3 (Shattil et al., 1987; BD), mouse anti-EGFP (Takara Bio Inc.), mouse anti-GFP (clone B2; Santa Cruz Biotechnology), mouse anti–β1 integrin (BD), mouse anti-GST (EMD Millipore), mouse anti-vinculin (Sigma-Aldrich), mouse anti–kindlin-2 (EMD Millipore), rabbit anti–kindlin-2 against C terminus of human K2 (Sigma-Aldrich), mouse anti–β-actin (clone 8H10D10; Cell Signaling Technology) antibody or with mouse anti-actin (clone AC-40, Sigma-Aldrich), and rabbit anti-FAK (Cell Signaling Technology). Secondary antibodies for Western blots were donkey anti–mouse HRP and goat anti–rabbit HRP (both from Santa Cruz Biotechnology). For confocal microscopy, detecting antibodies were Alexa Fluor 568 goat anti–rabbit Ig, Alexa Fluor 488 goat anti–mouse Ig, Alexa Fluor 488–phalloidin, Alexa Fluor 633–phalloidin, and Alexa Fluor 568–phalloidin (all from Life Technologies). For flow cytometry, Alexa Fluor 647 goat anti–mouse IgM was used to detect PAC1 binding (Jackson Immunoresearch). All other chemical reagents were analytical grade.

Plasmid construction, protein expression, and purification

For mammalian expression, full-length human K2, which was obtained from C. Wu (University of Pittsburgh, Pittsburgh, PA), was cloned in-frame into an EGFP C2 vector (Takara Bio Inc.; Ma et al., 2008) and talin-H domain (1–429 aa) into pDsRed-monomer (Bledzka et al., 2010). Point mutations were introduced into the K2 coding sequence using QuikChange site-directed mutagenesis system (Agilent Technologies). GST-fused full-length K2 and its mutants were expressed, purified, and quantified as described previously (Bledzka et al., 2010). In brief, GST-fused K2 and its mutants were expressed in *E. coli* BL21 cells (Agilent Technologies). The expressed proteins were purified using glutathione-Sepharose 4B resin followed by gel filtration on a HiLoad Superdex200 10/300 column (GE Healthcare). For selected experiments, the GST tag was enzymatically removed from the K2 by Factor Xa cleavage as described (Bledzka et al., 2012). The purified proteins were dialyzed against 50 mM Tris, pH 8.0, containing 150 mM NaCl, quantified using protein assay kits (Bio-Rad), and assessed for homogeneity by SDS-PAGE and their elution from the Superdex columns.

Pull-down, coimmunoprecipitation assays and Western blotting

Pull-down assays were performed using GST fusion proteins. Equal amounts of GST-fused K2 derivatives were added together with glutathione-Sepharose 4B to aliquots of the lysates of CHO, HUVEC, or HeLa cells or to purified actin. After 2 h at 4°C, the precipitates were collected by centrifugation, washed, and boiled in Laemmli sample buffer. The eluates were the analyzed on 4–20% gradient acrylamide gels under reducing conditions, and interactions of the actin with K2 were detected by Western blotting with mouse anti–β-actin. The gels were also stained with Coomassie blue to verify that sample loadings were similar. The transfer membranes were stained with Amido black.

SPR

Real-time protein–protein interactions were analyzed using a Biacore3000 instrument (Biacore). The surfaces of all flow cells were activated for 7 min with a 1:1 mixture of 0.1 M *N*-hydroxysuccinimide and 0.1 M 3-(*N*,*N*-dimethylamino)propyl-*N*-ethylcarbodiimide at a flow rate of 10 µl/min. Actin, myosin, or BSA was immobilized on CM5 biosensor chips using standard amine coupling chemistry with an injection of 10 µg/ml actin dissolved in Na acetate, pH 4.5, to reach the same coating density. Next, all surfaces were blocked with a 7-min injection of 1 M ethanolamine, pH 8.0. After completion of the immobilization procedure, the chip surface was stabilized in 10 mM Hepes, pH 7.4, containing 150 mM NaCl, 0.005% surfactant P20, and 0.2 mM $CaCl_2$. Experiments were performed at RT in 10 mM Hepes buffer, pH 7.4, containing 150 mM NaCl, 0.005% surfactant P20, and 0.2 mM $CaCl_2$ at a flow rate of 25 µl/min. SPR sensograms were obtained by injecting various concentrations of the K2 analyte. Injections were performed simultaneously over all four channels (three flow cells having different proteins immobilized and one flow cell with a blank surface as a control), and each concentration of analyte was tested in duplicate.

The association phases were followed for 2, 7, or 12 min at a flow rate of 25 µl/min, and dissociation phases were monitored for 5, 10, or 15 min. The chip surfaces were regenerated between consecutive binding cycles by injecting a short pulse of 10 mM NaOH and

stabilized for 1 min. The curves of the mock runs (buffer only) and of the blank flow cell were subtracted from their corresponding analyte binding curves. The resulting sensograms were analyzed in overlay plots using BIAevaluation software (version 4.01; GE Healthcare). The data were fitted to various models available in the global data analysis option, including a simple 1:1 Langmuir interaction model. The deviations of the SPR curves from a 1:1 model were quantified with the BIAevaluation software as the χ^2 parameter. χ^2 values >10% of the maximal deflection (R_{max}) were considered to indicate a poor fit of the data to the 1:1 Langmuir model. Binding responses in the steady-state region of the sensograms were also plotted against K2 protein concentration to estimate a relative dissociation constant.

Kindlin2 binding to immobilized actin in microtiter plate assays

The wells of microtiter plates (Corning Costar) were coated with actin (Cytoskeleton) at 0.3 or 2 µg/ml in a coating buffer of 0.2 M carbonate–bicarbonate, pH 9.4, for 20 h at 4°C and blocked with 3% BSA in GAB (5 mM Tris-HCl, pH 8.0, and 0.2 mM $CaCl_2$) for 1 h at 37°C. GST, GST-K2, either WT or mutant (0–1.5 µM), were added to the wells in GAB and incubated for 3 h at RT. Plates were washed with GAB, and bound GST proteins were detected by an ELISA using anti-GST mAb (GE Healthcare), peroxidase-conjugated secondary antibody (EMD Millipore), and 1-StepUltra TMB-ELISA (Thermo Fisher Scientific) as the substrate. The reaction was stopped by adding 1N HCl, and absorbance at 450 nm was measured. Assays were conducted in duplicate or triplicate, and the mean absorbance value at each K2 concentration was plotted after subtraction of the nonspecific absorption (determined as the difference between the signal of GST-K2 and GST). Binding responses were analyzed using Sigma Plot software (SPSS), in which the data were fitted to a one-site binding equation.

K2:actin cosedimentation assays

Actin binding to K2 was evaluated using Protein Spin-Down Biochem kits (Cytoskeleton, Inc.) according to the manufacturer's instructions. In brief, actin was resuspended to 1 mg/ml in general actin buffer (final concentrations 5 mM Tris-HCl, pH 8.0, and 0.2 mM $CaCl_2$) and left on ice for 30 min. Actin was polymerized by addition of 1:10 actin polymerization buffer (final concentrations 50 mM KCl, 2 mM $MgCl_2$, and 1 mM ATP) for 1 h at RT, producing 21 µM F-actin stock. Test proteins were centrifuged before use at 150,000 *g* at 4°C for 90 min (final concentration of proteins was 2–4 µM), incubated with the polymerized F-actin for 30 min, and centrifuged at 150,000 *g* at 24°C for 90 min. The supernatants and pellets were resuspended and boiled in SDS-containing sample buffer and analyzed on SDS-PAGE on 4–20% gradient acrylamide gels under reducing conditions.

Fluorescence microscopy of actin filaments

The influence of K2 on actin was evaluated by light microscopy using bacterial expressed K2 proteins that had been cleaved from their GST tags. Rabbit skeletal muscle actin (Cytoskeleton, Inc.) was hydrated in 5 mM Tris-HCl, 0.2 mM $CaCl_2$, 0.2 mM ATP, and 0.5 mM DTT, pH 8.0, overnight and centrifuged at 150,000 *g* at 4°C for 20 min; the supernatant was diluted to an actin concentration of 4 µM. Rabbit muscle actin (Cytoskeleton, Inc.) at 4 µM in 5 mM Tris-HCl, pH 8.0, and 0.2 mM $CaCl_2$, alone or in the presence of K2 proteins at a concentration of 1 or 6 µM, was polymerized by addition of polymerization buffer (final concentrations 50 mM KCl, 2 mM $MgCl_2$, and 1 mM ATP). The mixture was incubated for 60 min at 37°C. Before observation, the samples were diluted 1:10 into buffer containing 70 nM Alexa Fluor 488–phalloidin and applied to a coverslip coated with poly-L-lysine (0.01%). The effects of K2 on actin organization and Alexa Fluor 488–phalloidin staining were visualized by fluorescence light microscopy on a Leica DM5000B upright microscope (Leica Microsystems), using a Retiga SRV Cooled CCD camera (QImaging) and ImagePro Plus software (Media Cybernetics).

Cell culture and transfections

The murine myoblast cell line (C2C12) and the Chinese hamster ovary cell line stably expressing αIIbβ3 (CHO-A5) were cultured in high-glucose DMEM, DMEM-CUST, or DMEM:F12 with 10% FBS at 37°C in 5% CO_2. The human ovarian carcinoma cell line (OVCAR-3) was cultured in RPMI 1640 with 20% FBS and 0.01 mg/ml insulin. The cells were passaged using 0.05% trypsin/0.53 mM EDTA for dissociation at ∼80% confluence for CHO-A5 and OVCAR-3 cells or 40–50% for C2C12 cells. MAE cells were isolated from aortas of WT and $K2^{+/-}$ mice as described (Mahabeleshwar et al., 2006; Pluskota et al., 2011). For vector transfections into OVCAR-3 and CHOA5 cells, Lipofectamine 2000 (Life Technologies) was used. For siRNA transfections or rescue experiments in which K2 forms were expressed in C2C12 cells after siRNA knockdown, cells were nucleofected with kit V (Lonza) and program B-032. MISSION single siRNA specific for mouse K2 was obtained from Sigma-Aldrich. Specific assays were performed 24 h after transfection.

Immunofluorescence and cell spreading assays

Cell spreading assays were performed with MAE, C2C12, and OVC AR-3 cells. The cells were either untransfected or transiently transfected for 24 h and allowed to adhere and spread on vitronectin-coated (2.5 µg/ml) or fibronectin-coated (20 µg/ml) glass coverslips. After incubation at 37°C for selected times, the coverslips were washed three times with PBS, and the adherent cells were fixed with 4% paraformaldehyde and stained with Alexa Fluor–phalloidin (Life Technologies). As controls, untransfected cells were included in each experiment. For ILK and K2 localization in C2C12 cells, cells were costained with anti-vinculin monoclonal antibody, followed by Alexa Fluor 568–conjugated $F(ab')_2$ anti-mouse IgG secondary antibody. The coverslips were mounted with ProLong Gold antifade reagent (Life Technologies). The positively stained cells were visualized at 40× or 63× using a TCS-NT laser scanning confocal microscope (Leica), using confocal software (Leica). Images shown are representative of at least three independent experiments. Cell areas were analyzed with ImageJ software.

Integrin αIIbβ3 activation assays

Integrin αIIbβ3 activation was evaluated using PAC-1, a mAb specific for the activated conformation of this integrin (Shattil et al., 1985), as previously described (Ma et al., 2008). In brief, talin-H domain tagged with DsRed monomer or EGFP-tagged K2 and its mutants were expressed in CHO-A5 cells by transient transfection using Lipofectamine 2000 (Life Technologies). PAC-1 binding to the different transfectants (EGFP and DsRed double-positive cells) was analyzed by flow cytometry after incubating the transfected cells with 10 µg/ml anti-PAC1 mAb in HBSS buffer containing 0.1% BSA, 0.5 mM $CaCl_2$, and 0.5 mM $MgCl_2$ for 30 min at RT followed by fixation with 1% paraformaldehyde for 10 min at RT, washing, and incubation with 5 µg/ml Alexa Fluor 647–conjugated $F(ab')_2$ anti-mouse IgM secondary antibody for 30 min on ice. PAC-1 binding was analyzed on a LSR Fortessa flow cytometer (BD). Integrin activation was quantified as an activation index calculated using the following formula: 100 × (MFI – MFI of empty vector)/(MFI of maximal PAC-1 binding in the cells treated with 3 mM Mn^{2+} – MFI of empty vector), where MFI is the mean fluorescence intensity. To consider whether expression of various constructs in the αIIbβ3 CHO-A5 cells affected surface expression levels of the integrin, we evaluated reactivity with mAb 2G12, which reacts with αIIbβ3 independently of its activation state (Woods et al., 1986). Surface expression of αIIbβ3 varied by <10% among all transfectants.

Statistical analysis

Means and standard errors are reported. Statistical analyses using a two-tailed Student's *t* tests were performed in SigmaPlot (version 11). Differences were considered to be significant with $P < 0.05$.

Online supplemental material

Fig. S1 A shows that expression of FAK, vinculin, and β1 integrin is not changed after K2 knockdown in C2C12 cells by Western blot. Fig. S1 B shows surface expression of β1 after K2 knockdown in C2C12 cells by flow cytometry. Fig. S2 presents distribution of EGFP-tagged ILK in C2C12 cells after K2 knockdown. Fig. S3 presents representative SPR binding profiles of K2 and K2LK^{47}/AA mutant binding to an actin-coated chip, a BSA-coated chip, or a blank chip before subtracting of background controls. Fig. S4 shows K2 and K2LK^{47}/AA binding to actin coated onto microtiter plates. Fig. S5 A presents the levels of K2 variants expressed in transfected C2C12 cells after knockdown of endogenous K2. Fig. S5 B shows EGFP-tagged K2LK^{47}/AA mutant in C2C12 cells after K2 knockdown. Fig. S5 C shows the expression levels of kindlin-1, -2, and -3 in OVCAR-3 and BT-549 cells by Western blot. Online supplemental material is available at http://www.jcb.org/cgi/content/full/jcb.201501006/DC1.

Acknowledgments

We thank D. Szpak and X. Zhang for technical assistance. We thank Dr. K. Trybus and P.B. Joel of the University of Vermont College of Medicine for the baculovirus encoding the nonpolymerizable G-actin mutant and their advice on its purification.

This work was supported by National Institutes of Health grant P01HL073311 to E.F. Plow and J. Qin. HUVECs were provided by a grant awarded to Clinical and Translational Science Collaborative of Cleveland, a grant from the National Center for Advancing Translational Sciences (UL1TR000439) component of the National Institutes of Health, and National Institutes of Health Roadmap for Medical Research.

The authors declare no competing financial interests.

Submitted: 2 January 2015
Accepted: 22 February 2016

References

Algrain, M., O. Turunen, A. Vaheri, D. Louvard, and M. Arpin. 1993. Ezrin contains cytoskeleton and membrane binding domains accounting for its proposed role as a membrane-cytoskeletal linker. *J. Cell Biol.* 120:129–139. http://dx.doi.org/10.1083/jcb.120.1.129

Ali, R.H., and A.A. Khan. 2014. Tracing the evolution of FERM domain of Kindlins. *Mol. Phylogenet. Evol.* 80:193–204. http://dx.doi.org/10.1016/j.ympev.2014.08.008

Bandyopadhyay, A., G. Rothschild, S. Kim, D.A. Calderwood, and S. Raghavan. 2012. Functional differences between kindlin-1 and kindlin-2 in keratinocytes. *J. Cell Sci.* 125:2172–2184. http://dx.doi.org/10.1242/jcs.096214

Bialkowska, K., Y.Q. Ma, K. Bledzka, K. Sossey-Alaoui, L. Izem, X. Zhang, N. Malinin, J. Qin, T. Byzova, and E.F. Plow. 2010. The integrin co-activator Kindlin-3 is expressed and functional in a non-hematopoietic cell, the endothelial cell. *J. Biol. Chem.* 285:18640–18649. http://dx.doi.org/10.1074/jbc.M109.085746

Bledzka, K., K. Bialkowska, H. Nie, J. Qin, T. Byzova, C. Wu, E.F. Plow, and Y.Q. Ma. 2010. Tyrosine phosphorylation of integrin beta3 regulates kindlin-2 binding and integrin activation. *J. Biol. Chem.* 285:30370–30374. http://dx.doi.org/10.1074/jbc.C110.134247

Bledzka, K., J. Liu, Z. Xu, H.D. Perera, S.P. Yadav, K. Bialkowska, J. Qin, Y.Q. Ma, and E.F. Plow. 2012. Spatial coordination of kindlin-2 with talin head domain in interaction with integrin β cytoplasmic tails. *J. Biol. Chem.* 287:24585–24594. http://dx.doi.org/10.1074/jbc.M111.336743

Bretscher, A. 1983. Purification of an 80,000-dalton protein that is a component of the isolated microvillus cytoskeleton, and its localization in nonmuscle cells. *J. Cell Biol.* 97:425–432. http://dx.doi.org/10.1083/jcb.97.2.425

Dinkel, H., K. Van Roey, S. Michael, N.E. Davey, R.J. Weatheritt, D. Born, T. Speck, D. Krüger, G. Grebnev, M. Kuban, et al. 2014. The eukaryotic linear motif resource ELM: 10 years and counting. *Nucleic Acids Res.* 42(D1):D259–D266. http://dx.doi.org/10.1093/nar/gkt1047

Dowling, J.J., E. Gibbs, M. Russell, D. Goldman, J. Minarcik, J.A. Golden, and E.L. Feldman. 2008a. Kindlin-2 is an essential component of intercalated discs and is required for vertebrate cardiac structure and function. *Circ. Res.* 102:423–431. http://dx.doi.org/10.1161/CIRCRESAHA.107.161489

Dowling, J.J., A.P. Vreede, S. Kim, J. Golden, and E.L. Feldman. 2008b. Kindlin-2 is required for myocyte elongation and is essential for myogenesis. *BMC Cell Biol.* 9:36. http://dx.doi.org/10.1186/1471-2121-9-36

Feng, C., Y.F. Li, Y.H. Yau, H.S. Lee, X.Y. Tang, Z.H. Xue, Y.C. Zhou, W.M. Lim, T.C. Cornvik, C. Ruedl, et al. 2012. Kindlin-3 mediates integrin αLβ2 outside-in signaling, and it interacts with scaffold protein receptor for activated-C kinase 1 (RACK1). *J. Biol. Chem.* 287:10714–10726. http://dx.doi.org/10.1074/jbc.M111.299594

Friederich, E., K. Vancompernolle, C. Huet, M. Goethals, J. Finidori, J. Vandekerckhove, and D. Louvard. 1992. An actin-binding site containing a conserved motif of charged amino acid residues is essential for the morphogenic effect of villin. *Cell.* 70:81–92. http://dx.doi.org/10.1016/0092-8674(92)90535-K

Fukuda, K., K. Bledzka, J. Yang, H.D. Perera, E.F. Plow, and J. Qin. 2014. Molecular basis of kindlin-2 binding to integrin-linked kinase pseudokinase for regulating cell adhesion. *J. Biol. Chem.* 289:28363–28375. http://dx.doi.org/10.1074/jbc.M114.596692

Gary, R., and A. Bretscher. 1995. Ezrin self-association involves binding of an N-terminal domain to a normally masked C-terminal domain that includes the F-actin binding site. *Mol. Biol. Cell.* 6:1061–1075. http://dx.doi.org/10.1091/mbc.6.8.1061

Gingras, A.R., N. Bate, B.T. Goult, L. Hazelwood, I. Canestrelli, J.G. Grossmann, H. Liu, N.S. Putz, G.C. Roberts, N. Volkmann, et al. 2008. The structure of the C-terminal actin-binding domain of talin. *EMBO J.* 27:458–469. http://dx.doi.org/10.1038/sj.emboj.7601965

Gingras, A.R., N. Bate, B.T. Goult, B. Patel, P.M. Kopp, J. Emsley, I.L. Barsukov, G.C. Roberts, and D.R. Critchley. 2010. Central region of talin has a unique fold that binds vinculin and actin. *J. Biol. Chem.* 285:29577–29587. http://dx.doi.org/10.1074/jbc.M109.095455

Hamilton, T.C., R.C. Young, W.M. McKoy, K.R. Grotzinger, J.A. Green, E.W. Chu, J. Whang-Peng, A.M. Rogan, W.R. Green, and R.F. Ozols. 1983. Characterization of a human ovarian carcinoma cell line (NIH:OVCAR-3) with androgen and estrogen receptors. *Cancer Res.* 43:5379–5389.

He, Y., P. Esser, V. Schacht, L. Bruckner-Tuderman, and C. Has. 2011. Role of kindlin-2 in fibroblast functions: Implications for wound healing. *J. Invest. Dermatol.* 131:245–256. http://dx.doi.org/10.1038/jid.2010.273

Hemmings, L., D.J. Rees, V. Ohanian, S.J. Bolton, A.P. Gilmore, B. Patel, H. Priddle, J.E. Trevithick, R.O. Hynes, and D.R. Critchley. 1996. Talin contains three actin-binding sites each of which is adjacent to a vinculin-binding site. *J. Cell Sci.* 109:2715–2726.

Honda, S., H. Shirotani-Ikejima, S. Tadokoro, Y. Tomiyama, and T. Miyata. 2013. The integrin-linked kinase-PINCH-parvin complex supports integrin αIIbβ3 activation. *PLoS One.* 8:e85498. http://dx.doi.org/10.1371/journal.pone.0085498

Huet-Calderwood, C., N.N. Brahme, N. Kumar, A.L. Stiegler, S. Raghavan, T.J. Boggon, and D.A. Calderwood. 2014. Differences in binding to the ILK complex determines kindlin isoform adhesion localization and integrin activation. *J. Cell Sci.* 127:4308–4321. http://dx.doi.org/10.1242/jcs.155879

Janot, M., A. Audfray, C. Loriol, A. Germot, A. Maftah, and F. Dupuy. 2009. Glycogenome expression dynamics during mouse C2C12 myoblast differentiation suggests a sequential reorganization of membrane glycoconjugates. *BMC Genomics.* 10:483. http://dx.doi.org/10.1186/1471-2164-10-483

Jobard, F., B. Bouadjar, F. Caux, S. Hadj-Rabia, C. Has, F. Matsuda, J. Weissenbach, M. Lathrop, J.F. Prud'homme, and J. Fischer. 2003. Identification of mutations in a new gene encoding a FERM family protein with a pleckstrin homology domain in Kindler syndrome. *Hum. Mol. Genet.* 12:925–935. http://dx.doi.org/10.1093/hmg/ddg097

Joel, P.B., P.M. Fagnant, and K.M. Trybus. 2004. Expression of a nonpolymerizable actin mutant in Sf9 cells. *Biochemistry.* 43:11554–11559. http://dx.doi.org/10.1021/bi048899a

Kuijpers, T.W., E. van de Vijver, M.A. Weterman, M. de Boer, A.T. Tool, T.K. van den Berg, M. Moser, M.E. Jakobs, K. Seeger, O. Sanal, et al. 2009. LAD-1/variant syndrome is caused by mutations in FERMT3. *Blood.* 113:4740–4746. http://dx.doi.org/10.1182/blood-2008-10-182154

Larjava, H., E.F. Plow, and C. Wu. 2008. Kindlins: Essential regulators of integrin signalling and cell-matrix adhesion. *EMBO Rep.* 9:1203–1208. http://dx.doi.org/10.1038/embor.2008.202

Lee, H.S., R.M. Bellin, D.L. Walker, B. Patel, P. Powers, H. Liu, B. Garcia-Alvarez, J.M. de Pereda, R.C. Liddington, N. Volkmann, et al. 2004. Characterization of an actin-binding site within the talin FERM domain. *J. Mol. Biol.* 343:771–784. http://dx.doi.org/10.1016/j.jmb.2004.08.069

Liao, Z., H. Kato, M. Pandey, J.M. Cantor, A.J. Ablooglu, M.H. Ginsberg, and S.J. Shattil. 2015. Interaction of kindlin-2 with integrin β3 promotes outside-in signaling responses by the αVβ3 vitronectin receptor. *Blood.* 125:1995–2004. http://dx.doi.org/10.1182/blood-2014-09-603035

Liu, J., K. Fukuda, Z. Xu, Y.Q. Ma, J. Hirbawi, X. Mao, C. Wu, E.F. Plow, and J. Qin. 2011. Structural basis of phosphoinositide binding to kindlin-2 protein pleckstrin homology domain in regulating integrin activation. *J. Biol. Chem.* 286:43334–43342. http://dx.doi.org/10.1074/jbc.M111.295352

Liu, Y., Y. Zhu, S. Ye, and R. Zhang. 2012. Crystal structure of kindlin-2 PH domain reveals a conformational transition for its membrane anchoring and regulation of integrin activation. *Protein Cell.* 3:434–440. http://dx.doi.org/10.1007/s13238-012-2046-1

Ma, Y.Q., J. Qin, C. Wu, and E.F. Plow. 2008. Kindlin-2 (Mig-2): A co-activator of beta3 integrins. *J. Cell Biol.* 181:439–446. http://dx.doi.org/10.1083/jcb.200710196

Mahabeleshwar, G.H., P.R. Somanath, and T.V. Byzova. 2006. Methods for isolation of endothelial and smooth muscle cells and in vitro proliferation assays. *Methods Mol. Med.* 129:197–208.

Malinin, N.L., L. Zhang, J. Choi, A. Ciocea, O. Razorenova, Y.-Q. Ma, E.A. Podrez, M. Tosi, D.P. Lennon, A.I. Caplan, et al. 2009. A point mutation in KINDLIN3 ablates activation of three integrin subfamilies in humans. *Nat. Med.* 15:313–318. http://dx.doi.org/10.1038/nm.1917

Malinin, N.L., E.F. Plow, and T.V. Byzova. 2010. Kindlins in FERM adhesion. *Blood.* 115:4011–4017. http://dx.doi.org/10.1182/blood-2009-10-239269

Metcalf, D.G., D.T. Moore, Y. Wu, J.M. Kielec, K. Molnar, K.G. Valentine, A.J. Wand, J.S. Bennett, and W.F. DeGrado. 2010. NMR analysis of the alphaIIb beta3 cytoplasmic interaction suggests a mechanism for integrin regulation. *Proc. Natl. Acad. Sci. USA.* 107:22481–22486. http://dx.doi.org/10.1073/pnas.1015545107

Meves, A., C. Stremmel, K. Gottschalk, and R. Fässler. 2009. The Kindlin protein family: New members to the club of focal adhesion proteins. *Trends Cell Biol.* 19:504–513. http://dx.doi.org/10.1016/j.tcb.2009.07.006

Montanez, E., S. Ussar, M. Schifferer, M. Bösl, R. Zent, M. Moser, and R. Fässler. 2008. Kindlin-2 controls bidirectional signaling of integrins. *Genes Dev.* 22:1325–1330. http://dx.doi.org/10.1101/gad.469408

Mory, A., S.W. Feigelson, N. Yarali, S.S. Kilic, G.I. Bayhan, R. Gershoni-Baruch, A. Etzioni, and R. Alon. 2008. Kindlin-3: A new gene involved in the pathogenesis of LAD-III. *Blood.* 112:2591. http://dx.doi.org/10.1182/blood-2008-06-163162

Pakkanen, R., K. Hedman, O. Turunen, T. Wahlström, and A. Vaheri. 1987. Microvillus-specific Mr 75,000 plasma membrane protein of human choriocarcinoma cells. *J. Histochem. Cytochem.* 35:809–816. http://dx.doi.org/10.1177/35.8.3298422

Perera, H.D., Y.Q. Ma, J. Yang, J. Hirbawi, E.F. Plow, and J. Qin. 2011. Membrane binding of the N-terminal ubiquitin-like domain of kindlin-2 is crucial for its regulation of integrin activation. *Structure.* 19:1664–1671. http://dx.doi.org/10.1016/j.str.2011.08.012

Plow, E.F., J. Meller, and T.V. Byzova. 2014. Integrin function in vascular biology: A view from 2013. *Curr. Opin. Hematol.* 21:241–247. http://dx.doi.org/10.1097/MOH.0000000000000042

Pluskota, E., J.J. Dowling, N. Gordon, J.A. Golden, D. Szpak, X.Z. West, C. Nestor, Y.Q. Ma, K. Bialkowska, T. Byzova, and E.F. Plow. 2011. The integrin coactivator kindlin-2 plays a critical role in angiogenesis in mice and zebrafish. *Blood.* 117:4978–4987. http://dx.doi.org/10.1182/blood-2010-11-321182

Qadota, H., D.G. Moerman, and G.M. Benian. 2012. A molecular mechanism for the requirement of PAT-4 (integrin-linked kinase (ILK)) for the localization of UNC-112 (kindlin) to integrin adhesion sites. *J. Biol. Chem.* 287:28537–28551. http://dx.doi.org/10.1074/jbc.M112.354852

Qu, H., Y. Tu, X. Shi, H. Larjava, M.A. Saleem, S.J. Shattil, K. Fukuda, J. Qin, M. Kretzler, and C. Wu. 2011. Kindlin-2 regulates podocyte adhesion and fibronectin matrix deposition through interactions with phosphoinositides and integrins. *J. Cell Sci.* 124:879–891. http://dx.doi.org/10.1242/jcs.076976

Rogalski, T.M., G.P. Mullen, M.M. Gilbert, B.D. Williams, and D.G. Moerman. 2000. The UNC-112 gene in *Caenorhabditis elegans* encodes a novel component of cell-matrix adhesion structures required for integrin localization in the muscle cell membrane. *J. Cell Biol.* 150:253–264. http://dx.doi.org/10.1083/jcb.150.1.253

Roman, I., J. Figys, G. Steurs, and M. Zizi. 2006. Direct measurement of VDAC-actin interaction by surface plasmon resonance. *Biochim. Biophys. Acta.* 1758:479–486. http://dx.doi.org/10.1016/j.bbamem.2006.03.019

Rozario, T., P.E. Mead, and D.W. DeSimone. 2014. Diverse functions of kindlin/fermitin proteins during embryonic development in *Xenopus laevis*. *Mech. Dev.* 133:203–217. http://dx.doi.org/10.1016/j.mod.2014.07.004

Schaller, M.D. 2001. Paxillin: A focal adhesion-associated adaptor protein. *Oncogene.* 20:6459–6472. http://dx.doi.org/10.1038/sj.onc.1204786

Shattil, S.J., J.A. Hoxie, M. Cunningham, and L.F. Brass. 1985. Changes in the platelet membrane glycoprotein IIb.IIIa complex during platelet activation. *J. Biol. Chem.* 260:11107–11114.

Shattil, S.J., M. Cunningham, and J.A. Hoxie. 1987. Detection of activated platelets in whole blood using activation-dependent monoclonal antibodies and flow cytometry. *Blood.* 70:307–315.

Shi, X., Y.Q. Ma, Y. Tu, K. Chen, S. Wu, K. Fukuda, J. Qin, E.F. Plow, and C. Wu. 2007. The MIG-2/integrin interaction strengthens cell-matrix adhesion and modulates cell motility. *J. Biol. Chem.* 282:20455–20466. http://dx.doi.org/10.1074/jbc.M611680200

Svensson, L., K. Howarth, A. McDowall, I. Patzak, R. Evans, S. Ussar, M. Moser, A. Metin, M. Fried, I. Tomlinson, and N. Hogg. 2009. Leukocyte adhesion deficiency-III is caused by mutations in KINDLIN3 affecting integrin activation. *Nat. Med.* 15:306–312. http://dx.doi.org/10.1038/nm.1931

Tseng, Y., K.M. An, O. Esue, and D. Wirtz. 2004. The bimodal role of filamin in controlling the architecture and mechanics of F-actin networks. *J. Biol. Chem.* 279:1819–1826. http://dx.doi.org/10.1074/jbc.M306090200

Tsukita, S., Y. Hieda, and S. Tsukita. 1989. A new 82-kD barbed end-capping protein (radixin) localized in the cell-to-cell adherens junction: purification and characterization. *J. Cell Biol.* 108:2369–2382. http://dx.doi.org/10.1083/jcb.108.6.2369

Tu, Y., Y. Huang, Y. Zhang, Y. Hua, and C. Wu. 2001. A new focal adhesion protein that interacts with integrin-linked kinase and regulates cell adhesion and spreading. *J. Cell Biol.* 153:585–598. http://dx.doi.org/10.1083/jcb.153.3.585

Tu, Y., S. Wu, X. Shi, K. Chen, and C. Wu. 2003. Migfilin and Mig-2 link focal adhesions to filamin and the actin cytoskeleton and function in cell shape modulation. *Cell.* 113:37–47. http://dx.doi.org/10.1016/S0092-8674(03)00163-6

Turunen, O., T. Wahlström, and A. Vaheri. 1994. Ezrin has a COOH-terminal actin-binding site that is conserved in the ezrin protein family. *J. Cell Biol.* 126:1445–1453. http://dx.doi.org/10.1083/jcb.126.6.1445

Ussar, S., H.V. Wang, S. Linder, R. Fässler, and M. Moser. 2006. The Kindlins: subcellular localization and expression during murine development. *Exp. Cell Res.* 312:3142–3151. http://dx.doi.org/10.1016/j.yexcr.2006.06.030

Ussar, S., M. Moser, M. Widmaier, E. Rognoni, C. Harrer, O. Genzel-Boroviczeny, and R. Fässler. 2008. Loss of Kindlin-1 causes skin atrophy and lethal neonatal intestinal epithelial dysfunction. *PLoS Genet.* 4:e1000289. http://dx.doi.org/10.1371/journal.pgen.1000289

Vardar, D., D.A. Buckley, B.S. Frank, and C.J. McKnight. 1999. NMR structure of an F-actin-binding 'headpiece' motif from villin. *J. Mol. Biol.* 294:1299–1310. http://dx.doi.org/10.1006/jmbi.1999.3321

White, S.J., and W.H. McLean. 2005. Kindler surprise: Mutations in a novel actin-associated protein cause Kindler syndrome. *J. Dermatol. Sci.* 38:169–175. http://dx.doi.org/10.1016/j.jdermsci.2004.12.026

Woods, V.L. Jr., L.E. Wolff, and D.M. Keller. 1986. Resting platelets contain a substantial centrally located pool of glycoprotein IIb-IIIa complex which may be accessible to some but not other extracellular proteins. *J. Biol. Chem.* 261:15242–15251.

Xu, Z., X. Chen, H. Zhi, J. Gao, K. Bialkowska, T.V. Byzova, E. Pluskota, G.C. White II, J. Liu, E.F. Plow, and Y.Q. Ma. 2014. Direct interaction of kindlin-3 with integrin αIIbβ3 in platelets is required for supporting arterial thrombosis in mice. *Arterioscler. Thromb. Vasc. Biol.* 34:1961–1967. http://dx.doi.org/10.1161/ATVBAHA.114.303851

Xue, Z.H., C. Feng, W.L. Liu, and S.M. Tan. 2013. A role of kindlin-3 in integrin αMβ2 outside-in signaling and the Syk-Vav1-Rac1/Cdc42 signaling axis. *PLoS One.* 8:e56911. http://dx.doi.org/10.1371/journal.pone.0056911

Ye, F., B.G. Petrich, P. Anekal, C.T. Lefort, A. Kasirer-Friede, S.J. Shattil, R. Ruppert, M. Moser, R. Fässler, and M.H. Ginsberg. 2013. The mechanism of kindlin-mediated activation of integrin αIIbβ3. *Curr. Biol.* 23:2288–2295. http://dx.doi.org/10.1016/j.cub.2013.09.050

Zhu, L., J. Hatakeyama, C. Chen, A. Shastri, K. Poon, and J.G. Forte. 2008. Comparative study of ezrin phosphorylation among different tissues: More is good; too much is bad. *Am. J. Physiol. Cell Physiol.* 295:C192–C202. http://dx.doi.org/10.1152/ajpcell.00159.2008